Angewandte Chemie International Edition

Angewandte International Edition Chemie

How to cite: *Angew. Chem. Int. Ed.* **2026**, e1434064
doi.org/10.1002/anie.1434064

RESEARCH ARTICLE

Structure-Encoded Oxidation Enables Nucleotide-Resolved RNA Editing, Conjugation, and Structural Probing

Jieyi Shentu | Ziyi Jiang | Qilong Tan | Linglan Fang

Department of Chemistry, School of Science and Research Center For Industries of the Future, Zhejiang Key Laboratory of Precise Synthesis of Functional Molecules, Westlake University, Hangzhou, Zhejiang, P. R. China

Correspondence: Linglan Fang (fanglinglan@westlake.edu.cn)

Received: 28 March 2026 | **Revised:** 15 April 2026 | **Accepted:** 25 April 2026

Keywords: bioconjugation | oxidation | posttranscriptional modification | RNA structure

ABSTRACT

RNA oxidation is pervasive in stress and disease biology and has also been harnessed in chemical biology through proximity labeling, ligand-directed photochemistry, and oxidative RNA targeting. In most settings, the regioselectivity is specified by spatial proximity or a specialized RNA-binding ligand, and the resulting modification is typically distributed across a local region rather than at a designated nucleotide. Here we show that, with selected oxidants, RNA secondary structure can itself serve as a programmable handle to control RNA oxidation site-selectively. We define practical structure–reactivity rules that determine which guanosine is oxidized and which lesions predominate, based on loop geometry and oxidant identity. Guided by these rules, we develop LOCAL (Localized Oxidation Constrained at Loops), a DNA-programmed, postsynthetic method that directs guanosine oxidation to predetermined sites in transcribed RNAs with nucleotide-resolved selectivity. LOCAL enables oxidative base editing to modulate RNA interactions and stability, provides a plug-and-play tool for site-specific bioconjugation via nucleophile trapping of oxidized guanosines, and serves as a blue-light-gated, guanosine-focused structural readout of RNA single-strandedness and ligand-induced structural changes. Together, these results position RNA oxidation as a nucleotide-resolved, structure-encoded reaction manifold that complements existing ligand-encoded oxidative targeting chemistry, and 2′-OH- and enzyme-based RNA chemistries.

1 | Introduction

RNA-reactive chemistries are central tools for modifying and interrogating RNA in vitro and in cells [1], and there is growing interest in reactions that can be directed with nucleotide-level precision. Widely used reaction manifolds include 2′-hydroxyl acylation (SHAPE reagents) [2–4], nucleobase *N*-alkylation (e.g., dimethyl sulfate) [5], and more recent acetonylation chemistry [6], which together enable site-resolved labeling, control of RNA function, and profiling of RNA structure and interactions [7–9]. DNA-directed strategies, such as RNA Acylation at Induced Loops (RAIL), further demonstrate that complementary oligonucleotides can program local RNA architecture and thereby direct reactivity to selected nucleotides [10]. These advances illustrated a broad paradigm that RNA structure can be exploited as a programmable handle for chemical reactivity. Oxidation is especially attractive in this regard, because it creates distinctive modifications with direct consequences for RNA folding, recognition, and fate. However, compared to other RNA-reactive chemistries, general methods to direct oxidation to a predetermined nucleotide remain comparatively underdeveloped, which otherwise likely open new applications complementary to existing RNA chemistries.

Previous studies have nevertheless established important precedent for localized RNA oxidation. Photosensitizers and

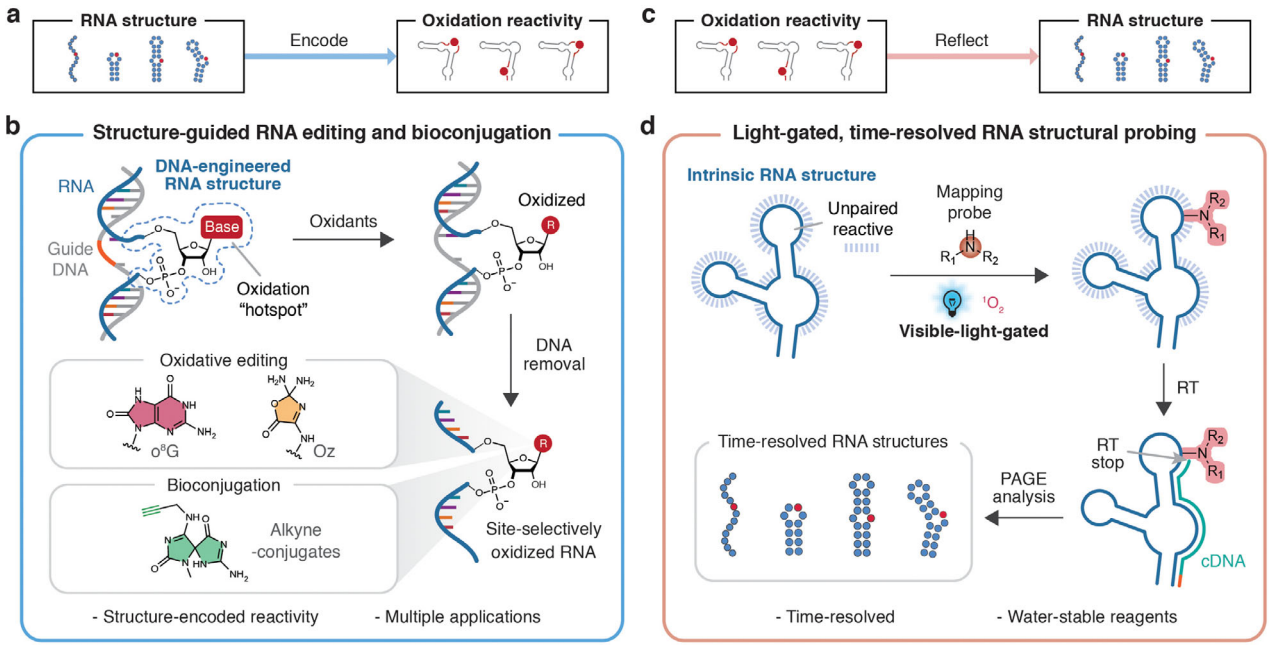

FIGURE 1 | Structure-encoded oxidation enables site-selective RNA editing, bioconjugation, and structural probing. (a) An illustration showing RNA structures encode the oxidation reactivity of RNA. (b) Workflow of structure-guided RNA editing and bioconjugation. Complementary DNAs reinforce duplex protection and DNA-engineered loop structures direct guanosine oxidation (o^8G or Oz) or bioconjugation "handles" to user-defined sites on transcribed RNAs. (c) An illustration showing the oxidative reactivity in turn reflects RNA structural information. (d) Workflow of light-gated, time-resolved RNA structure probing via oxidative labeling. Unpaired Gs can be rapidly and selectively labeled via singlet oxygen-mediated oxidative labeling, enabling time-resolved analysis of RNA secondary structures.

redox-active reagents have been used for proximity labeling and RNA manipulation [11–13]. Moreover, oxidation has also been made programmable through molecular recognition. A seminal example is ligand-directed photochemical oxidation by Grate and Wilson, who engineered a malachite green (MG) binding motif into an mRNA to trigger localized photochemical inactivation of the targeted RNA [14]. More recently, small-molecule recognition has been used to recruit oxidants or radical-generating molecules to specific RNA motifs. RNA-binding ligands containing Ru^{3+} complexes can promote localized RNA oxidation, driving targeted RNA cleavage in cells and animals [15–17]. Studies on toxic RNA repeats have further shown that, when a suitable recognition motif is present, small molecules can be used for selective crosslinking and cleavage of RNA [18].

These studies show that ligand-encoded RNA oxidation can be localized, programmable, and biologically consequential. Meanwhile, because targeting is achieved by ligand–RNA recognition, the reactive regions are typically defined by the neighborhood of the binding ligand. As a result, they often cause region-specific oxidation or cleavage rather than at a single designated nucleotide. Although powerful when a recognition motif is present, these elegant approaches may not be readily generalizable to other arbitrary sites. This motivated us to explore a different targeting principle. Instead of using ligand binding to confine oxidation within a region, we wondered whether programmed RNA structures could more precisely pinpoint which nucleotides are reactive and which are inert, thus enhancing both the resolution and generality of RNA oxidation.

Here, we present a structure-encoded strategy by which the oxidative hotspot is specified by the local RNA geometry with nucleotide-level precision, imposed by a short guide DNA rather than ligand recognition of a pre-existing RNA motif. We use guide DNAs to impose predictable local RNA structures that convert a designated nucleotide into an oxidation "hotspot" while flanking helices remain protected (Figure 1a,b). We first derive structure–reactivity rules in RNA–DNA hybrids, showing that small DNA-engineered bulges and loops strongly enhance oxidation, and that oxidant identity determines the primary lesion (8-oxoguanosine o^8G or oxazolone Oz) (Figure 1b). Guided by these rules, we developed LOCAL (Localized Oxidation Constrained at Loops), a DNA-programmed, postsynthetic platform that directs guanosine oxidation to specific RNA nucleotides with nucleotide-level resolution. We then show that this same structure-encoded oxidation can underpin three applications that previously required disparate tools: nucleotide-resolved oxidative, enzyme-free bioconjugation, and blue-light-gated, guanosine-focused structural probing of RNA single-strandedness and ligand-induced conformational changes (Figure 1c,d). Thus, LOCAL complements ligand-encoded oxidative targeting and established 2′-OH and enzyme-based RNA chemistries.

2 | Results and Discussion

2.1 | RNA Secondary Structure as a Handle for Site-Selective Guanosine Oxidation

To turn RNA secondary structure into a practical control element for site-selective oxidation, we first sought to define structure–reactivity relationships and identify oxidative regimes that strongly discriminate paired and unpaired sequences. We envision that with proper oxidants, if base-paired RNA duplexes

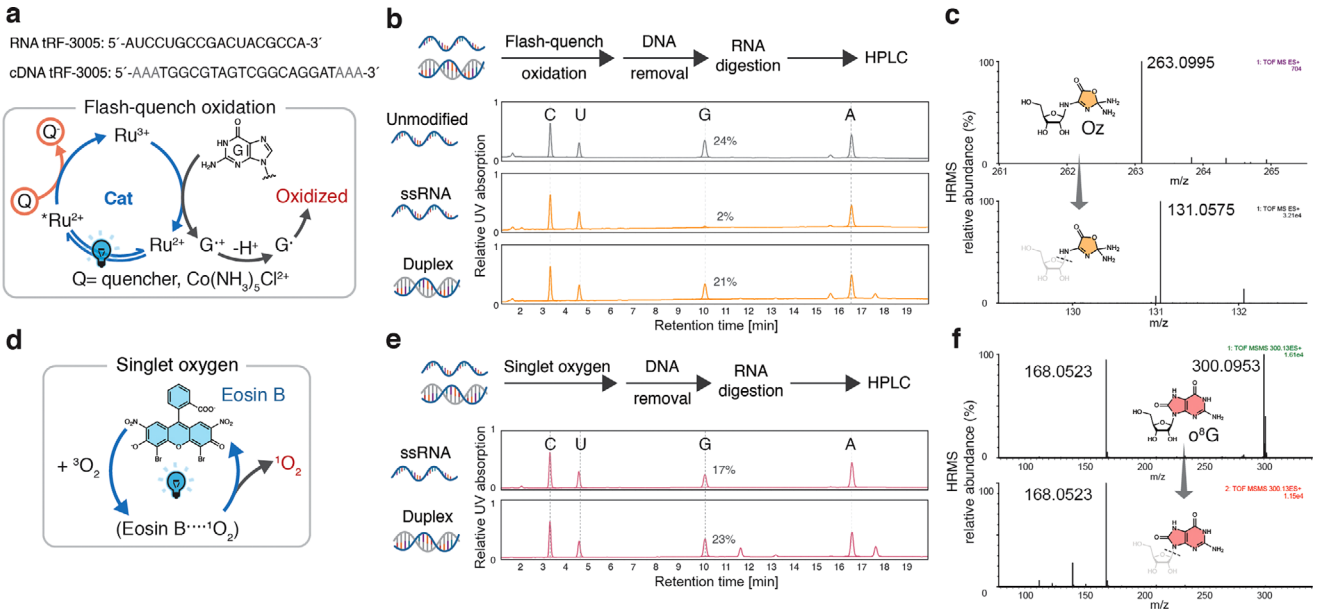

FIGURE 2 | RNA secondary structure as a handle for site-selective guanosine oxidation. (a) Top: Sequences of model RNA and cDNA. Bottom: Mechanisms of RNA oxidation by $Ru(bpy)_3^{2+}$ and the quencher $Co(NH_3)_5Cl^{2+}$ via the flash-quench method. (b) HPLC analysis of digested nucleosides of ssRNA and RNA–DNA duplex upon flash-quench oxidation. The UV absorption was measured at 254 nm. (c) Representative high-resolution mass spectrometry (HRMS) showing that G in ssRNA is predominantly oxidized to Oz by flash-quench oxidation under the tested condition. (d) Generation of singlet oxygens by photosensitizer Eosin B upon blue-light irradiation. (e) HPLC analysis of digested nucleosides upon oxidation with singlet oxygens. Relative UV absorption is calculated as the percentage of the peak area out of the sum of C/U/G/A peaks. The additional minor peaks observed in HPLC traces are from the residue of digested cDNA rather than oxidation products (Figure S6). (f) HRMS analysis showing that G in ssRNA is predominantly oxidized to o^8G by singlet oxygens under the tested condition.

are shielded to oxidation whereas the unpaired regions remain reactive, then complementary DNAs could be used to protect most of the RNA in a duplex with oxidation confined to engineered, solvent-exposed loops, thereby gating oxidation reactivity with secondary structure rather than sequence alone (Figure S1).

To test this, we compared single-stranded versus RNA-DNA duplex under two mechanistically distinct oxidative regimes (Figure 2). We used an 18-nt single-stranded tRNA-derived fragment tRF-3005 that contains multiple G residues in varied sequence contexts. Complementary DNAs were designed with three 5′ and 3′-deoxyadenosines to stabilize the duplex termini via A_3 dangling ends (Figure 2a), which has been shown to enhance helix formation via stacking effects [19]. After annealing, RNAs were subjected either to flash-quench oxidation with $Ru(bpy)_3^{2+}$/ $Co(NH_3)_5Cl^{2+}$ under blue light or to singlet oxygen oxidation with Eosin B as a photosensitizer (Figure 2a–c,d–f). In each case, reacted RNA was recovered after DNase treatment, and nucleoside composition and backbone integrity were analyzed by HPLC, high-resolution mass spectrometry, and gel electrophoresis.

To avoid off-target oxidation by photocatalysts that can intercalate with duplexes, we employed a well-characterized non-intercalating photocatalyst, $Ru(bpy)_3^{2+}$, under flash-quench conditions [20]. In this way, oxidation is primarily determined by solvent accessibility; thus, paired, inaccessible Gs are protected from oxidation. Under flash-quench conditions, single-stranded RNA (ssRNA) was highly susceptible to guanosine oxidation: HPLC analysis showed a ~92% loss of G, whereas A/C/U remained largely unchanged (Figure 2b). High-resolution mass spectrometry identified oxazolone (Oz) as the predominant product (Figures 2c and S2), consistent with prior reports of flash-quench-mediated guanine oxidation, where o^8G is initially formed and subsequently undergoes further oxidation in the presence of $Co(NH_3)_5Cl^{2+}$[21–23], and denaturing gels revealed extensive backbone scission (Figure S3). In sharp contrast, the corresponding RNA-DNA duplex exhibited minimal G consumption by HPLC. It retained nearly intact full-length RNA under identical conditions (Figures 2b and S3a), indicating that base-paired helices are strongly protected from both nucleobase oxidation and strand cleavage by this oxidant.

We next asked whether this structure-dependent reactivity extends to a chemically distinct oxidant that yields different products (Figure 2d–f). Singlet oxygen is well documented to oxidize guanine, with 8-oxoguanosine (o^8G) as a major detectable base lesion under reported conditions [24, 25]. Treating single-stranded model RNA with Eosin B and blue light led to partial consumption of G within ssRNA and formation of o^8G as the predominant detectable guanine oxidation product under our conditions (Figures S4 and S5). Again, the RNA-DNA duplex was markedly more oxidation-resistant, with only minor G consumption was detected and strand integrity was almost completely preserved (Figures 2e and S3a).

Across these experiments, two trends emerge. First, under tested conditions, both $Ru(bpy)_3^{2+}$/ $Co(NH_3)_5Cl^{2+}$ and Eosin B-derived singlet oxygen preferentially oxidize unpaired, solvent-exposed Gs, while largely sparing Gs and backbones embedded in RNA-DNA helices. Second, the identity of the oxidant determines the

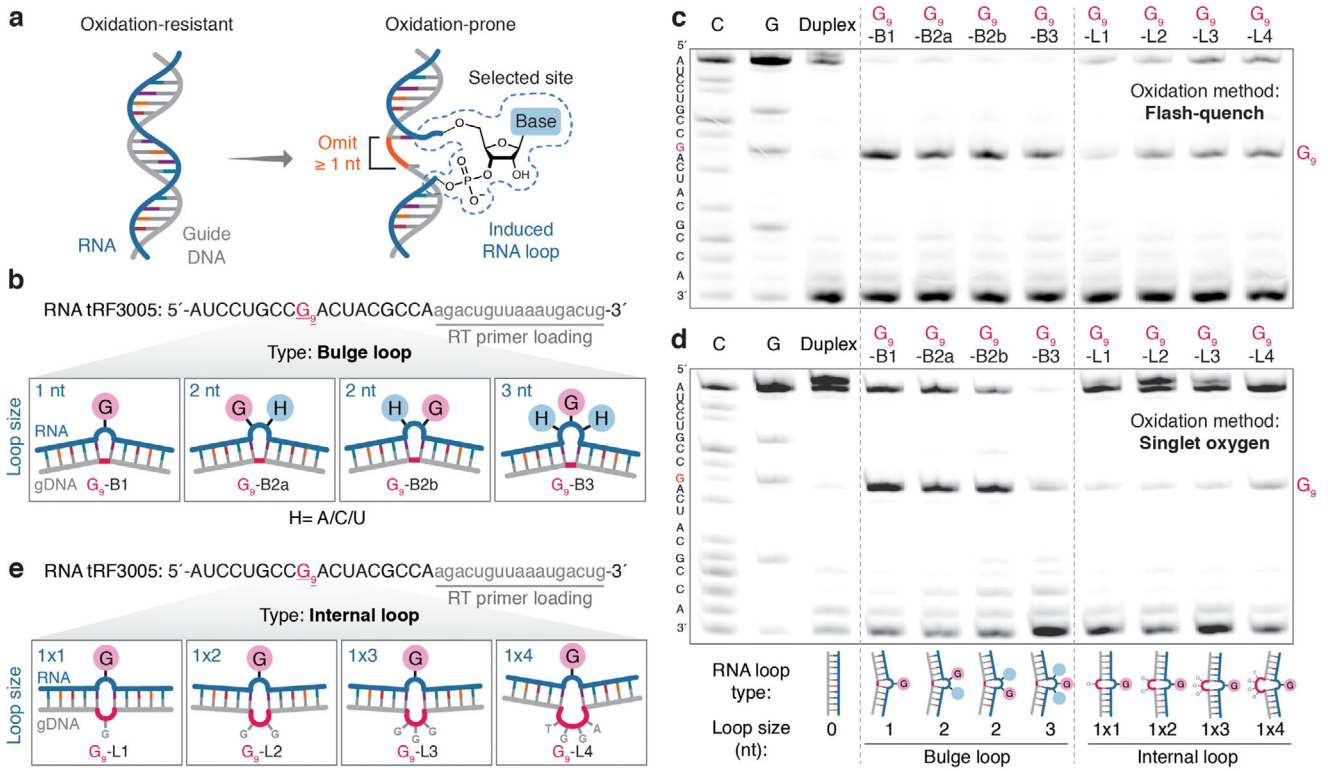

FIGURE 3 | Engineered RNA loops program the position of oxidative modification. (a) An illustration of RNA–DNA hybrids exposing unpaired bulge loops for oxidation. (b) A set of guide DNAs induces a 1- to 3-nt bulge loop at a prescribed site in model RNA tRF-3005. Guide DNAs contain ≥ 1 ribonucleotide omitted at the sites of interest. B1, B2, and B3 represent 1-, 2-, and 3-nt bulge loops, respectively. (c, d) Representative PAGE gel showing premature termination of reverse transcription (RT) at oxidized sites. The RNA was preannealed with different bulge loop (left)- and internal loop (right)-inducing DNAs. The RNA–DNA hybrids were treated under flash-quench conditions (c) or oxidized by singlet oxygen (d). For (c) and (d), the lane markers C and G indicate the corresponding nucleotide in RNA. The targeted guanine G_9 is highlighted in red. (e) Guide DNAs induce 1 × 1, 1 × 2, 1 × 3, and 1 × 4 internal loops at G_9 of tRF3005 RNA. See uncropped images in the Supporting Information.

dominant product (Oz vs. o^8G), providing a simple way to vary the chemical form of installed oxidative product without later changing the guiding architecture. These observations suggest a basic structure–reactivity framework that duplex formation suppresses guanosine oxidation and unpaired regions serve as oxidation-prone elements. We will later extend this principle to loop elements engineered by guide DNAs, asking whether unpaired loop motifs can localize G oxidation to selected positions in otherwise protected RNA.

2.2 | Engineered RNA Loops Program the Position of Oxidative Modification

Our duplex-protection experiments suggested an overall design logic; that is, under selected oxidative regimes, paired helices are difficult to oxidize, whereas unpaired regions are oxidation-prone. We therefore asked whether small, engineered RNA loops could be used to introduce discrete oxidation "hotspots" within otherwise protected RNA-DNA duplexes and, in doing so, provide a practical solution for positioning oxidative modifications (Figure 3a).

We first tested whether a minimal bulge loop is sufficient to convert a protected G into a highly reactive site. Guide DNAs with a single-nucleotide deletion opposite to G_9 in tRF-3005 generated a 1-nt bulge loop, while 2- to 3-nt deletions form larger bulges (Figure 3b). Under flash-quench conditions that strongly oxidize unpaired Gs, heteroduplexes bearing a 1-nt bulge yielded a dominant band that corresponds to the primer-extension stop immediately 3′ of G_9 (ca. >∼95% conversion), while the RNA backbone remained intact (Figures 3c and S3b). A fully complementary duplex under identical conditions showed little to no modification at G_9 under the flash-quench condition. Notably, stop bands observed during primer-extension analysis are most likely caused by stalled reverse transcriptases at oxidized RNA bases, in accordance with previous reports [26, 27]. Consistent with these findings, Burrows et al. reported that SuperScript III also led to stop bands at sites containing oxidative lesions, including o^8G, as well as fully extended cDNA products [28]. Likewise, under singlet-oxygen conditions that moderately oxidize unpaired Gs, a 1-nt bulge loop also provides effective modification at G_9 (Figure 3d). Notably, Gs within the bulge loops appear to be more reactive than those within ssRNA (Figure 2e), suggesting the likelihood of loops promoting oxidation via unknown mechanisms. Thus, a single 1-nt bulge appears sufficient to convert an otherwise protected G into an oxidation hotspot.

Next, we examined how loop geometry and position within the loop influence reactivity. We found that increasing the bulge size from 1-nt to 3-nt preserved the reaction "hotspot" at G_9 but

slightly reduced overall yield (Figure 3c,d), indicating a trade-off between loop size and oxidation efficiency. Within dinucleotide bulges, placing G at the 3′ portions of the loop consistently yielded stronger oxidation than placing it at the 5′ side, likely due to the unpaired loop nucleobases at the 5′ end potentially adopting a more stacked-in conformation with reduced reactivity (Figure S7). Internal loops, constructed by inserting one or more unpaired G nucleotides opposite to G_9 in the guide DNA (internal loop type: 1 × 1, 1 × 2, 1 × 3, 1 × 4), also supported localized oxidation under both flash-quench and singlet oxygen conditions, but with a drastically decreased level of modification than the 1-nt bulge (Figures 3c,d and S8). Taken together, these data suggest a structural hierarchy for reactivity under our oxidative regimes: 1-nt bulge > 2- to 3-nt bulge > internal loop > duplexes, with 3′ residues in small bulges being seemingly more reactive than their 5′ counterparts.

With these rules in hand, we tested whether the position of oxidation could be programmed simply by moving the loop along the RNA. For this reason, we designed a panel of guide DNAs by which a 1-nt bulge can be shifted from G_9 to other G residues in tRF-3005 (Figure S9). For each guide DNA, flash-quench oxidation produced a dominant RT stop at the nucleotide immediately 3óf the targeted G, and this stop moves with the shifting loop, consistent with single-nucleotide positional control. Finally, to test whether multiple sites can be edited simultaneously, we designed a multitargeted guide DNA containing 1-nt deletions opposite to both G_6 and G_{15}, thereby generating two 1-nt bulges within the same duplex (Figure S10). Flash-quench oxidation produced strong RT stops at both positions (ca. ∼50%–94% conversion), indicating dual-site editing. Together, these results show that simple DNA-encoded loop motifs are sufficient to determine where guanosine oxidation occurs in RNA-DNA hybrids, and provide several design rules—including how loop geometry, size, and G position within the loop influence the reactivity—which we will later deploy in LOCAL to install oxidative modifications at user-defined sites for functional studies, bioconjugation, and structural probing.

2.3 | Site-Selective Oxidation Modulates RNA-Ligand Interaction and Exonuclease Decay

A key motivation for LOCAL is to move beyond phenotypes of bulk RNA oxidation and test how a specific oxidative modification at a defined site affects RNA function. Genetic mutations can identify critical bioregulatory sites, but cannot answer whether the chemistry of oxidation itself—including altered hydrogen-bonding, electrostatic interactions, and sugar pucker—is sufficient to rewire RNA function. With LOCAL, we can directly address this gap by installing defined oxidative modification at prescribed sites without changing sequences. We tested this idea on two fundamental RNA processes: small molecule–RNA interaction and exonucleolytic decay.

We first asked whether a single oxidation at a key binding-site guanosine is sufficient to disrupt small molecule-RNA interactions (Figure 4a). The MG aptamer is a well-characterized fluorogenic RNA whose response depends on a structured MG-binding pocket, with G_{23} as a part of a critical base triple (C_{10}–G_{23}–A_{27}) lining the ligand-binding pocket (Figure 4b) [29, 30]. Prior studies have shown that genetic mutations within this triple base element can partially weaken fluorogenicity [29], but the specific impact of oxidation at this position was unclear. Using LOCAL, we engineered a 1-nt bulge there and applied flash-quench oxidation to install the Oz modification at that site. Primer extension analysis confirmed efficient editing at G_{23} (Figure S11), which led to approximately 80% reduction in the fluorescence of MG-aptamer complex compared to the unmodified counterpart (Figure 4c,d). This suggests that oxidative modification perturbs the surrounding residues in ways that may not be fully mimicked by mutagenesis.

Furthermore, we evaluated the impacts of oxidized guanosine on RNA G-quadruplex (rG4) formation. We oxidized two representative G residues, G_8 and G_{11}, from two key tetrads located within a well-characterized 21-nt West Nile Virus (WNV) rG4 core via flash-quench oxidation (Figure S12a) [31]. To characterize the modification, we appended a primer-binding sequence to its 3′ end, and denaturing PAGE analysis confirmed selective and efficient oxidation at these two sites (Figure S12b). We found that oxidation at different G residues led to distinct structural impacts on the rG4, as the characteristic circular dichroism (CD) peak of rG4 at ∼268 nm was retained upon oxidation at either site. However, we did observe a modest reduction in the intensity of the characteristic peak in oxG_{11}-rG4, which further decreased upon oxidation of G_8 (Figure S12c). Thus, a single site-selective oxidative modification is sufficient to affect rG4 structure.

We next examined if different oxidative modifications at the same RNA site have comparable impacts on RNA decay (Figure 4e–g). The 5′-3′ exoribonuclease 1 (Xrn-1) degrades many cytoplasmic RNAs, and prior studies have shown that o^8G in RNA can stall Xrn-1, implicating oxidative modification in modulating RNA decay [32–34]. However, these analyses have largely focused on o^8G and have not directly compared distinct oxidative modifications at the same site in an otherwise identical RNA. Using LOCAL, we introduced either o^8G or Oz at G_9 of our model tRF-3005 RNA at a similar level (Figure 4e). Under enzymatic conditions where unmodified RNA was almost completely degraded by Xrn-1, RNAs bearing an o^8G at G_9 produced a stalled fragment consistent with Xrn-1 stalling at the modified site (Figure 4f,g), in agreement with previous reports [33, 34]. Notably, RNAs bearing an Oz at the same site produced a very similar stalled band, indicating that chemically distinct oxidative modifications of G, Oz, and o^8G, can both act as strong barriers to Xrn-1 when installed at a single defined site.

Taken together, LOCAL turns oxidative damages into site-selective perturbations. These results support the broader premise that RNA oxidation is not just a passive biomarker of stress, but can actively rewire RNA interactions and processing, and that LOCAL provides a practical way to test such effects one modification and one site at a time, which is otherwise difficult to address previously.

Loop-directed oxidation enables simple, site-selective RNA bioconjugation. Singlet oxygen-mediated guanosine oxidation followed by nucleophile trapping is already used in proximity-labeling methods to tag accessible G residues for enrichment and sequencing [35, 36]. In its usual form, however, this chemistry broadly labels exposed Gs proximal to the singlet oxygen genera-

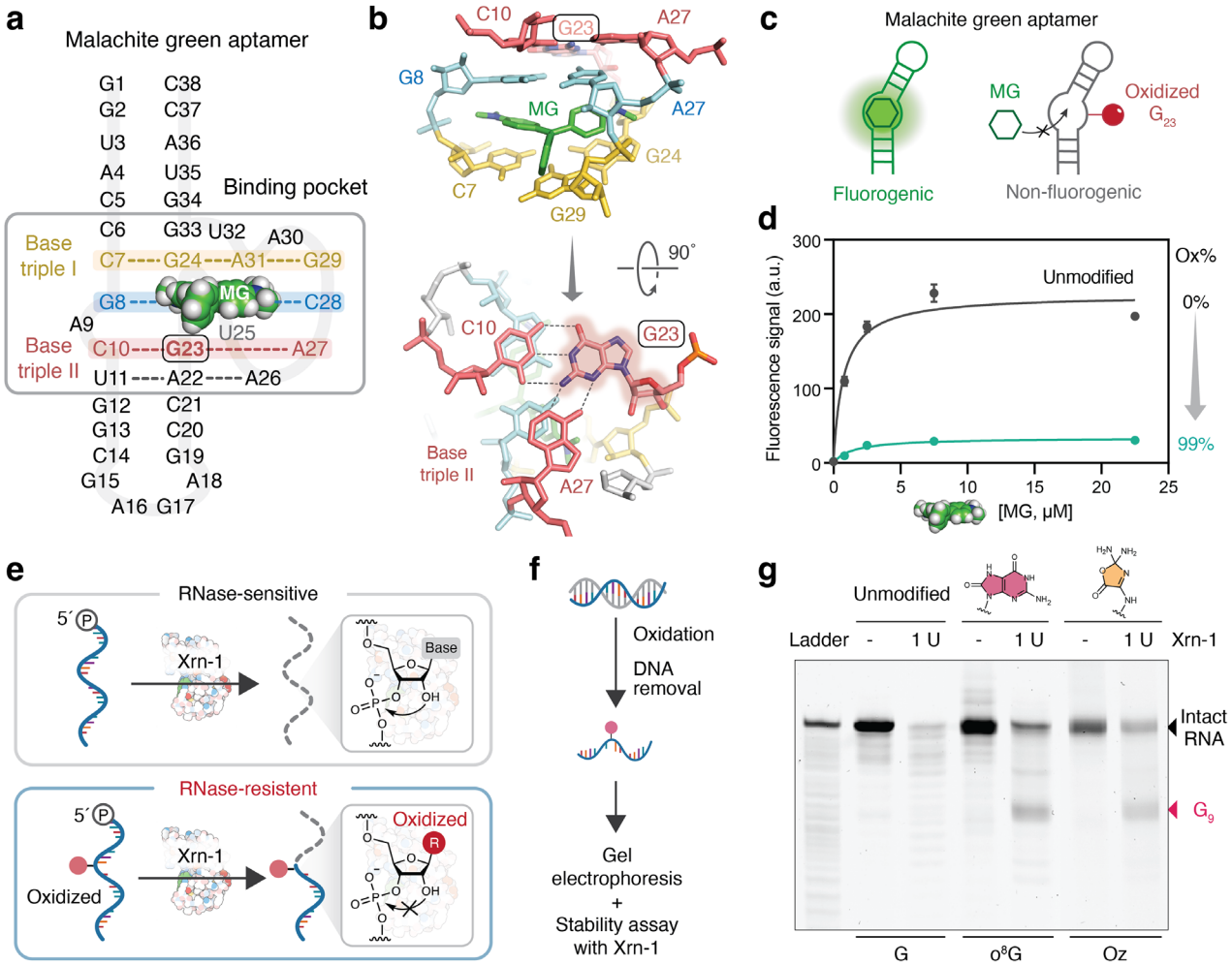

FIGURE 4 | Site-selective oxidation modulates RNA-ligand interaction and exonuclease decay. (a) An illustration of the sequence and structural features of malachite green (MG) aptamer. (b) MG is stacked between a base quadruple (C_7–G_{24}–G_{29}–A_{31}) and a Watson–Crick base pair (G_8–C_{28}) (top). A critical base triple (C_{10}–G_{23}–A_{27}) lines the edge of the MG binding pocket, where G_{23} (highlighted in box) interweaves the base triple via H-bonding with C_{10} and A_{27} (bottom). (c) Comparison of the fluorogenicity of the MG aptamer with or without oxidation at G_{23}. (d) Quantitative assessment of the fluorescence signal of wild-type and oxidized MG aptamer in the presence or absence of MG (one site-specific binding model). The data represent mean ± SEM, $n = 3$ independent experiments. (e) An illustration of RNA decay of unmodified RNA (top) or oxidized RNA (bottom) in the presence of 5′-exonuclease Xrn-1. (f) Workflow of RNA decay assay to characterize the enzymatic stability of 5′-phosphorylated tRF-3005 (35 nt) RNA in the presence of Xrn-1. (g) Representative denaturing PAGE analysis showing that Xrn-1 stalls upon encountering o^8G or Oz, while fully degrading the unmodified RNA. See uncropped images in the Supporting Information.

tors; it does not provide nucleotide-level selectivity. We reasoned that the same structural gating strategy that underpins LOCAL can, in principle, convert this bulk G-labeling reaction into a DNA-programmable, site-selective bioconjugation platform (Figure 5a).

As an initial test, we investigated whether a simple bulge loop could confine oxidative labeling to a pre-determined G residue. To test this, we paired a 37-nt model RNA with a guide DNA containing a single-nucleotide deletion opposite to G_9 to create a defined 1-nt bulge loop, and carried out singlet-oxygen oxidation in the presence of propargylamine (Figure S13a), which has been used for proximity-labeling of guanosines [36]. Primer extension showed a dominant RT stop immediately 3′ of G_9, and MALDI-TOF analysis was consistent with the addition of ~1 propargylamine adduct per RNA (Figure S13b,c). In contrast, a fully complementary guide DNA almost completely inhibited labeling, whereas unprotected RNA strand was extensively modified (median number of adducts ~3) (Figure S13c). Moreover, we extend this approach for site-selective labeling of a long GFP-mRNA (Figure S14). Tiling of 1031-nt GFP-mRNA by multiple guide DNAs that complements mRNA side-by-side effectively protects the long mRNA from modification, whereas 1-nt bulge led to sufficient labeling at prescribed site G_{887}. Together, our data show that an engineered 1-nt bulge is sufficient to confine nucleophile trapping to one guanosine for short and long RNAs, while the surrounding duplex remains largely inert, which is not attainable with the previous proximity-based labeling by single oxygen.

We then evaluated how loop position and geometry affect where the conjugation locates. Shifting the bulge along the RNA by redesigning the guide DNAs repositioned the predominant labeling site (Figure S15), reflecting the behavior seen for oxidative

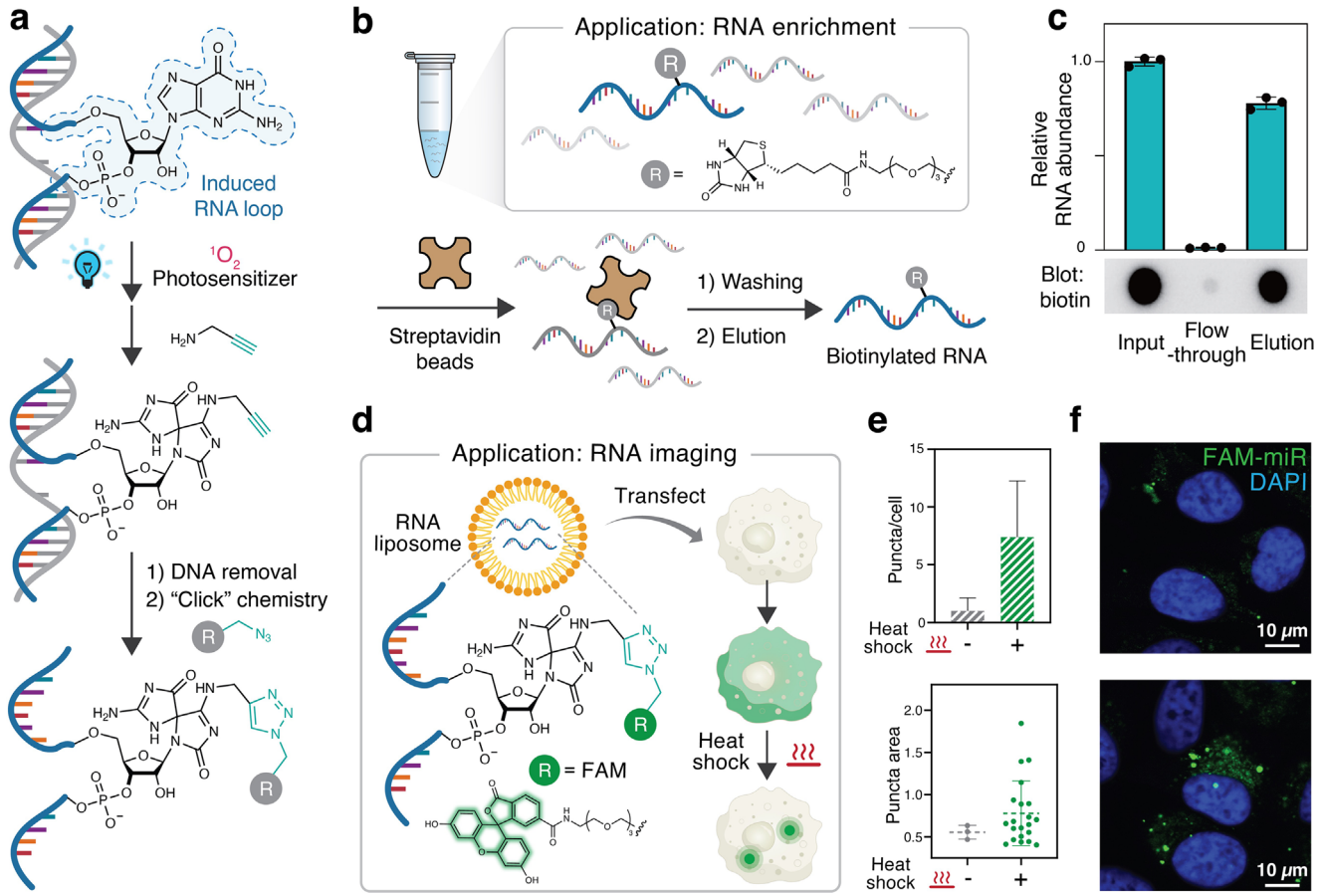

FIGURE 5 | Loop-directed oxidation enables simple, site-selective RNA bioconjugation. (a) Experimental workflow for site-selective bioconjugation of RNA via loop-constrained oxidation. The selected G within DNA-induced loops can be efficiently oxidized by singlet oxygens and subsequently "trapped" by propargylamine. The alkyne–RNA conjugates could then be further derivatized through copper-catalyzed "click" chemistry. (b) Workflow for enriching biotinylated RNA from a mixture of nucleic acids. (c) Top: Plot quantifying the level of enrichment of biotinylated miR-124. Bottom: Dot-blot analysis showing the enrichment of biotinylated RNA. The data represent mean ± SEM, $n = 3$ independent experiments. (d) Experimental workflow to image FAM-labeled RNA upon heat shock stress. Cells were lipofected with FAM-labeled miR-124, followed by heat shock at 42°C for 40 min. Data represent mean ± SEM, $n = 3$ independent experiments. (e) Plot comparing the number of fluorescent puncta per cell (top) and the area of puncta (bottom) before and after heat shock. Data represent mean ± SEM of 125 to 149 cells. (f) Representative fluorescence images of cells lipofected with FAM-labeled miR-124 before and after heat shock. Scale bar = 10 μm.

editing. When we introduced GG dinucleotide bulges, labeling appeared to favor the 3′ G (Figure S15a, $G_{11}G_{12}$–B2), consistent with the positional bias observed in the editing experiments. We also found that guide DNAs that create bulges adjacent to a weakly paired closing base U may produce collateral labeling at such bases (Figure S15a, G_{14}–B1), suggesting avoidance of U as closing bases for nucleotide-resolution labeling. These observations extend the structure–reactivity rules of LOCAL into the bioconjugation application: 1-nt bulges provide effective single-site labeling; labeling of larger bulges bias toward the 3′ G nucleobases; and weak closing base U should be avoided when high regioselectivity is required.

Finally, we tested whether LOCAL-derived handles operate as expected in standard enrichment and imaging workflows. Propargylamine-labeled RNAs were efficiently derivatized with a biotin-azide by copper-catalyzed alkyne–azide cycloaddition (CuAAC) "click" reactions [37, 38], captured almost stoichiometrically on streptavidin beads and recovered at ~80% yield upon denaturation (Figure 5b,c), supporting their use in pull-down applications. In another experiment, introducing a fluorescein (FAM) fluorophore into miR-124 via click chemistry produced diffuse cytoplasmic fluorescence in lipotransfected cells that condensed into puncta upon heat shock (Figures 5d–f and S15b,c), consistent with stress-induced relocation of microRNAs [39]. These examples do not introduce new click or imaging chemistry. However, they show that LOCAL's loop-directed oxidation can be coupled directly into existing CuAAC-based workflows to deliver site-selectively labeled RNAs without requiring specialized enzymes or pre-modified nucleotides. In this way, we turned a previously proximity-driven singlet oxygen/nucleophile labeling chemistry into a nucleotide-resolved, DNA-programmable bioconjugation tool.

2.4 | Light-Gated Oxidative Probing of RNA Secondary Structure

Chemical probing has been extensively used to map RNA secondary structure by evaluating 2′-OH and Watson-Crick face

reactivity, and highly reactive SHAPE and dimethyl sulfate reagents have enabled snapshots of RNA structures on the sub-minute timescale [5, 40, 41]. However, in most of these time-resolved methods, temporal resolution is hardwired into the hydrolytic lifetime of highly water-labile electrophiles such as BzCN, 1M7, or TMO that hydrolyze rapidly [40–42]. So, these reactions must be initiated by rapid mixing and probe's hydrolysis, rather than an external trigger, which determines the observation window. Moreover, Light Activated Structural Examination of RNA (LASER) uses UV-activated nitrenes to report on purine solvent accessibility, not classical base pairing [7, 8], and relies on UV irradiation with potential photodamage of RNA [43]. To our knowledge, there are no widely adopted methods that combine a SHAPE-like readout of RNA single-strandedness with gating by benign visible light rather than reagent hydrolysis or UV irradiation. We therefore asked whether the structure-dependent G oxidation that underpins LOCAL could be repurposed into a light-gated approach for secondary-structure probing, by which all reagents are stable in the dark and brief blue-light alone defines when structural information is recorded as covalent marks.

We first benchmarked our oxidative labeling against a widely used SHAPE reagent, 2-methylnicotinic acid imidazolide (NAI) [44], using the *Escherichia coli* flavin mononucleotide (FMN) riboswitch as a test case [45, 46] (Figure 6). As an initial test, under singlet-oxygen conditions with propargylamine trapping, we varied the duration of blue-light irradiation and compared the resulting RT-stop patterns with NAI on the same RNA. Approximately 15 s of irradiation already produced a robust pattern of G-focused RT stops, and 30 s yielded strong structural signals, whereas NAI required a 10-min incubation to reach comparable labeling levels (Figure 6a,b). Oxidative pattern distinguished unpaired from paired regions in a manner broadly consistent with SHAPE analysis but with signals concentrated at G (Figure 6c). In several regions, the oxidative probe showed stronger reactivity at unpaired sites than NAI under matched conditions, suggesting greater sensitivity at those sites. Moreover, prolonged irradiation over 30 s led to enriched RT termination bands towards the 3′ ends of RNA, with RT-stop signals diminishing from the 5′ ends of RNA (Figure S16), consistent with prolonged irradiation resulting in excessive modification that exceeds "single-hit" kinetic regime. Thus, brief irradiation of blue light is sufficient to infer G-focused secondary structure on a sub-minute timescale using water-stable reagents, complementing classical SHAPE structural profiles.

Mechanistically, singlet oxygen oxidation of G first generates an electrophilic guanosine lesion that can be intercepted by an external nucleophile to yield a stable G-adduct [35, 36, 48], which produces strong RT stops. For a fixed rate of oxidation, the choice of nucleophile might therefore tune labeling efficiency. To optimize this trapping step, we assembled a panel of nucleophilic probes with varied nucleophilicity, steric bulk, and aromaticity (Figure 7a). Screening revealed a trend: primary alkylamines provided the strongest structural signals, whereas even a single *N*-methyl substitution substantially abolished labeling, and more hindered or aromatic nucleophiles were generally ineffective. Probes with heteroatoms other than nitrogen at the nucleophilic sites also failed for effective trapping (Figure 7b). From this panel, we selected a smaller primary amine **1** and a bulkier one **3** for detailed comparison on the *apo* FMN riboswitch. Overall, probe **3** produced more RT stops and higher reactivity at many unpaired sites than **1**, consistent with more efficient trapping (Figure 7c). When we compare labeled sites by their local architecture, we observed a clear pattern; that is, in narrow (distance to the closest neighboring nucleotide < 3.35 Å), less solvent-exposed (solvent exposure < 60%) environments, two probes exhibited similar labeling efficiency, whereas **3** consistently outperformed **1** in roomier and more exposed spaces (Figures 7d,e and S17). These data suggest that the smaller probe can reach Gs in tight pockets that partially exclude the bulkier probes. Together, our data confirm that primary alkylamines are preferred trapping reagents, and demonstrate that probe size can be used to bias labeling toward more open versus more occluded structural environments.

We then asked whether this approach could provide biologically interpretable structural information in a well-defined regulatory RNA (Figure 7f–h). The FMN riboswitch is an ideal benchmark because its ligand-induced rearrangements around the FMN-binding pocket have been mapped in detail by x-ray crystallography [46, 49, 50] and are known to underpin its bioregulation of gene expression [46, 51]. Using a 30s blue-light irradiation window, we compared oxidative labeling profiles of the *apo* aptamer and the FMN-bound state. Upon FMN addition, multiple Gs around the binding pocket showed decreased reactivity, consistent with reduced intermolecular accessibility upon ligand engagement (Figure 7f,g). In contrast, several positions distal to the ligand-binding pocket became more reactive, which were located within regions exhibiting increased solvent-exposure (Figure 7g,h), consistent with local shielding near the pocket and broader structural rearrangements across the riboswitch upon ligand engagement. Taken together, these results repurpose RNA oxidation—previously implicated in RNA damage and spatial labeling—into a light-gated, sub-minute, structure-dependent labeling approach that can be adjusted to different local environments.

3 | Conclusion

Several lines of previous work laid the foundation of LOCAL. Proximity labeling showed that oxidation chemistry can be used to label RNAs within defined spatial neighborhoods [11–13]. Aptamer/MG-directed photooxidation showed that engineered ligand–RNA recognition can localize RNA inactivation to specific regions [14]. Small-molecule RNA binders linked to photosensitizers and other RNA-cleaving oxidants extended this principle to region-specific oxidation in cells and animals [15–18]. These elegant approaches encode oxidative targeting through ligand–RNA recognition, whose specificity is primarily determined by proximity-driven ROS diffusion, leaving room to advance from motif-specific to nucleotide-level selectivity. Thus, LOCAL adds a complementary design principle; that is, the site of oxidation is encoded by a DNA-imposed secondary structure that defines a single oxidation "hotspot," rather than by a highly specialized RNA-binding ligand or ligand-binding motif.

This difference is critical because it changes both the resolution and scope of RNA oxidation. In ligand-encoded approaches, the oxidant was recruited by ligand–RNA recognition, and thus the nucleotides in its neighborhood became reactive. These

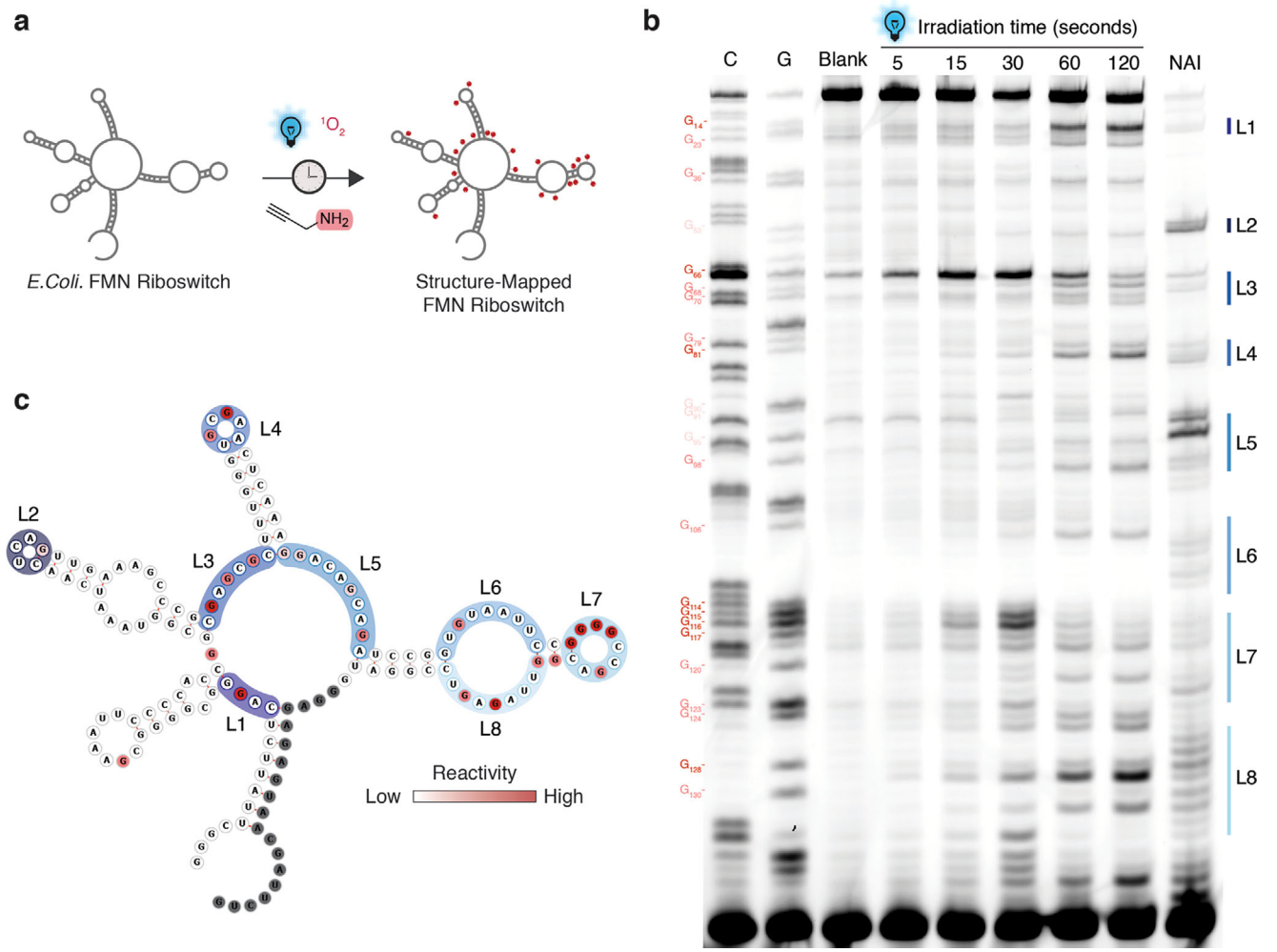

FIGURE 6 | Light-gated RNA structure mapping via oxidative labeling. (a) An illustration of structure mapping of the FMN riboswitch via light-gated oxidation. (b) Primer extension analysis showing both the extent and locations of oxidatively labeled G sites. Loop regions of the FMN riboswitch were labeled with 100 mM of a widely used SHAPE reagent (NAI) at 25°C for 10 min, which reacts with 2′-OH groups in flexible, single-stranded RNA segments. Sequencing lanes are labeled with C and G for nucleotide identification. (c) An illustration of secondary structure of the FMN riboswitch predicted by the RNAfold [47]. Oxidatively labeled G sites were colored with varying shades of red indicating their reactivity (based on data from panel b), and the primer binding sequence is colored gray. See uncropped images in the Supporting Information.

methods are powerful when a suitable recognition motif exists in RNA, but they are typically motif-restricted and not readily generalizable to arbitrary sites. As a result, the outcomes are often distributed RNA oxidation or cleavage within the targeted region. In contrast, we identified actionable structure–reactivity rules: small induced bulge loops act as oxidation hotspots, base-paired helices are strongly oxidation-resistant, and oxidant identity determines the predominant lesion (o^8G vs. Oz). It is important to note that the choice of oxidants is critical. As LOCAL's selectivity relies on differential reactivity between unpaired and paired sequences, promiscuous oxidants such as free radicals that cause substantial electron-hopping effects may be avoided. Thus, LOCAL primarily relies on outer-sphere electron transfer and singlet-oxygen pathways to maximize single-nucleotide resolution, and does not use classical oxidants such as intercalating bleomycin that generates free radicals [52]. These rules helped us design and install oxidative modifications at predesignated sites in transcribed RNAs with nucleotide-resolved selectivity. Nucleic acid hybridization can impose local structures and direct especially 2′-acylation reactivity in tools such as RAIL [10], and our present study effectively extends these concepts to oxidative chemistry.

Building on this structure-encoded oxidative reaction, the same structure–reactivity rule can support three applications that previously relied on disparate tools. LOCAL can perform site-selective oxidative base editing to modulate ligand–RNA interactions and RNA stability, enable nucleotide-resolved bioconjugation via trapping of oxidized guanosines with simple nucleophiles, and provide a blue-light-gated, guanosine-focused structural probing approach of RNA single-strandedness and ligand-induced conformational changes. A limitation of the present approach is its reliance on using multiple protector DNAs for modifying long RNAs (>300 nt), which might be addressed by developing DNA conjugates to catalyze oxidation locally. Together, these support RNA oxidation as a nucleotide-resolved, structure-encoded platform for RNA editing, bioconjugation, and light-gated structural probing, adding a distinct oxidative toolset alongside existing 2′-OH- and enzyme-based approaches for probing and manipulating RNAs with high precision.

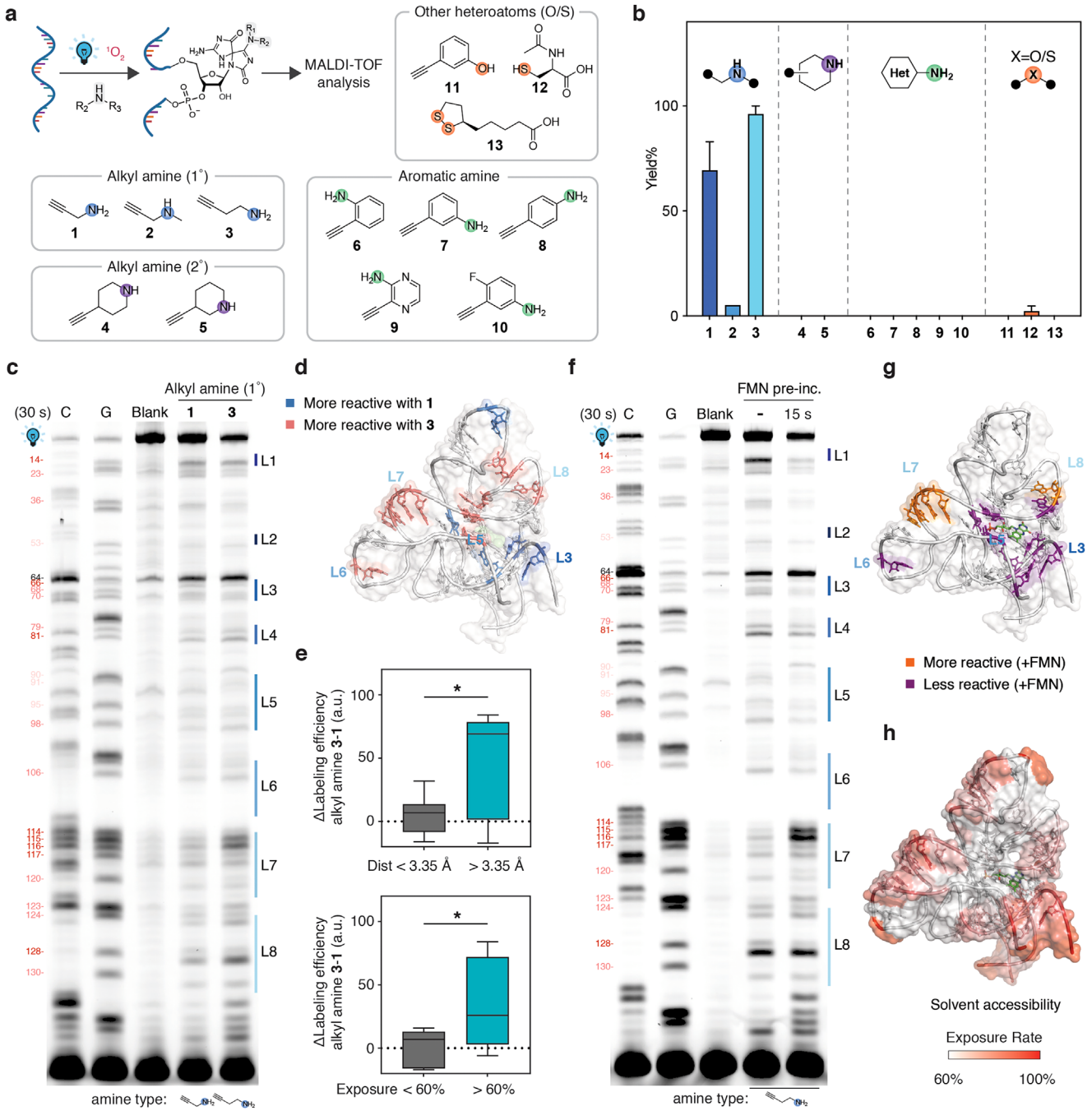

FIGURE 7 | Disparate trapping nucleophiles capture RNA structural changes in varied microenvironment. (a) Optimization of nucleophilic trapping reagents for oxidative labeling. The labeling efficiency was detected by MALDI-TOF analysis. (b) Bar graph comparing the labeling efficiency of tRF-3005 with different nucleophilic trapping reagents (**1** to **13**). All trapping reagents were tested at 20 mM. The data represent mean ± SEM, $n = 3$ independent experiments. (c) Primer extension analysis comparing the labeling patterns of alkyl amines **1** and **3**. The duration of blue-light-irradiation was uniformly set to 30 s. (d) Modeled structure of *E.* coli FMN riboswitch comparing the labeling patterns of **1** and **3**. Gs that are more reactive toward **1** are colored blue, whereas those more reactive towards **3** are colored red. (e) Top: A box plot comparing the labeling efficiency between **1** and **3** at Gs within tight or spacious spaces, where the closest atom distance to labeled G is less than or more than 3.35 Å. Bottom: A box plot comparing the labeling efficiency between **1** and **3** at sites with solvent exposure rate less than or more than 60%. *: p value < 0.05 (two-tailed t-test). (f) Primer extension analysis showing the reactivity pattern of FMN riboswitch with or without FMN ligand, using probe **3**. The duration of blue-light-irradiation was uniformly set to 30 s. (g) Modeled structure of FMN riboswitch was colored to highlight G residues exhibiting higher (orange) and lower (purple) oxidative labeling reactivity upon ligand engagement. (h) Structure of FMN riboswitch showing the solvent exposure rate that is color-coded using a gradient of red. See uncropped images in the Supporting Information.

Author Contributions

Jieyi Shentu: investigation, methodology, validation, visualization, writing – review and editing, formal analysis, data curation. **Ziyi Jiang**: data curation. **Qilong Tan**: resources. **Linglan Fang**: conceptualization, investigation, funding acquisition, writing – original draft, writing – review and editing, project administration, supervision, resources.

Acknowledgments

This project was supported by the Westlake University startup (to L. F.) and Zhejiang Provincial Natural Science Foundation of China under Grant Number LQKWL26B0701. We thank Dr. Yinjuan Chen from Instrumentation and Service Center for Molecular Sciences at Westlake University for the assistance in UPLC-TOFMS measurement. We thank Lingyu Xiao from Instrumentation and Service Center for Molecular Sciences at Westlake University for the supporting in cell imaging. We also thank Wenwen Zhang from Mass Spectrometry & Metabolomics Core Facility of Westlake University for MS analysis. Thanks for all the instrument support from the Instrumentation and Service Center for Molecular Sciences and the Mass Spectrometry & Metabolomics Core Facility of the Biomedical Research Core Facilities at Westlake University. We thank Dr. Xin Zhang and Dr. Lu Xiao for the useful discussion.

Conflicts of Interest

Westlake University has filed a patent application based on the methods described in this work, in which L. F. and J. S T. are named as inventors. The other authors declare no conflicts of interest.

Data Availability Statement

The data that support the findings of this study are available in the supplementary material of this article

References

1. R. C. Spitale and D. Incarnato, "Probing the Dynamic RNA Structurome and Its Functions," *Nature Reviews Genetics* 24 (2023): 178–196, https://doi.org/10.1038/s41576-022-00546-w.

2. J. L. McGinnis, J. A. Dunkle, J. H. Cate, and K. M. Weeks, "The Mechanisms of RNA SHAPE Chemistry," *Journal of the American Chemical Society* 134 (2012): 6617–6624, https://doi.org/10.1021/ja2104075.

3. E. J. Merino, K. A. Wilkinson, J. L. Coughlan, and K. M. Weeks, "RNA Structure Analysis at Single Nucleotide Resolution by Selective 2′-Hydroxyl Acylation and Primer Extension (SHAPE)," *Journal of the American Chemical Society* 127 (2005): 4223–4231, https://doi.org/10.1021/ja043822v.

4. R. C. Spitale, R. A. Flynn, Q. C. Zhang, et al., "Structural Imprints in Vivo Decode RNA Regulatory Mechanisms," *Nature* 519 (2015): 486–490, https://doi.org/10.1038/nature14263.

5. S. E. Wells, J. M. Hughes, A. H. Igel, and M. Ares Jr., "Use of Dimethyl Sulfate to Probe RNA Structure In Vivo," *Methods in Enzymology* 318 (2000): 479–493.PMID: 10890007.

6. Y. H. Lee, E. Yu, and C. M. Park, "Programmable Site-selective Labeling of Oligonucleotides Based on Carbene Catalysis," *Nature Communications* 12 (2021): 1681, https://doi.org/10.1038/s41467-021-21839-4.

7. C. Feng, D. Chan, J. Joseph, et al., "Light-Activated Chemical Probing of Nucleobase Solvent Accessibility inside Cells," *Nature Chemical Biology* 14 (2018): 276–283, https://doi.org/10.1038/nchembio.2548.

8. B. Zinshteyn, D. Chan, W. England, C. Feng, R. Green, and R. C. Spitale, "Assaying RNA Structure With LASER-Seq," *Nucleic Acids Research* 47 (2019): 43–55, https://doi.org/10.1093/nar/gky1172.

9. L. Xiao, L. Fang, and E. T. Kool, "2′-OH as a Universal Handle for Studying Intracellular RNAs," *Cell Chemical Biology* 31 (2024): 110–124, https://doi.org/10.1016/j.chembiol.2023.10.022.

10. L. Xiao, M. Habibian, and E. T. Kool, "Site-Selective RNA Functionalization via DNA-Induced Structure," *Journal of the American Chemical Society* 142 (2020): 16357–16363, https://doi.org/10.1021/jacs.0c06824.

11. K. L. Engel, H. G. Lo, R. Goering, Y. Li, R. C. Spitale, and J. M. Taliaferro, "Analysis of Subcellular Transcriptomes by RNA Proximity Labeling With Halo-seq," *Nucleic Acids Research* 50 (2022): e24, https://doi.org/10.1093/nar/gkab1185.

12. Y. Li, M. B. Aggarwal, K. Ke, K. Nguyen, and R. C. Spitale, "Improved Analysis of RNA Localization by Spatially Restricted Oxidation of RNA–Protein Complexes," *Biochemistry* 57 (2018): 1577–1581, https://doi.org/10.1021/acs.biochem.8b00053.

13. H. G. Lo, R. Goering, A. Kocere, et al., "Quantification of Subcellular RNA Localization Through Direct Detection of RNA Oxidation," *Nucleic Acids Research* 53 (2025): gkaf139.

14. D. Grate and C. Wilson, "Laser-Mediated, Site-Specific Inactivation of RNA Transcripts," *PNAS* 96 (1999): 6131–6136, https://doi.org/10.1073/pnas.96.11.6131.

15. L. Guan and M. D. Disney, "Small-Molecule-Mediated Cleavage of RNA in Living Cells," *Angewandte Chemie* 52 (2013): 1462–1465, https://doi.org/10.1002/anie.201206888.

16. L. Guan, Y. Luo, W. W. Ja, and M. D. Disney, "Small Molecule Alteration of RNA Sequence in Cells and Animals," *Bioorganic & Medicinal Chemistry Letters* 28 (2018): 2794–2796, https://doi.org/10.1016/j.bmcl.2017.10.034.

17. A. J. Angelbello, S. G. Rzuczek, K. K. McKee, et al., "Precise Small-Molecule Cleavage of an R(CUG) Repeat Expansion in a Myotonic Dystrophy Mouse Model," *PNAS* 116 (2019): 7799–7804, https://doi.org/10.1073/pnas.1901484116.

18. S. G. Rzuczek, L. A. Colgan, Y. Nakai, et al., "Precise Small-molecule Recognition of a Toxic CUG RNA Repeat Expansion," *Nature Chemical Biology* 13 (2017): 188–193, https://doi.org/10.1038/nchembio.2251.

19. N. Sugimoto, R. Kierzek, and D. H. Turner, "Sequence Dependence for the Energetics of Dangling Ends and Terminal Base Pairs in Ribonucleic Acid," *Biochemistry* 26 (1987): 4554–4558, https://doi.org/10.1021/bi00388a058.

20. A. M. Pyle, J. P. Rehmann, R. Meshoyrer, C. V. Kumar, N. J. Turro, and J. K. Barton, "Mixed-Ligand Complexes of Ruthenium(II): Factors Governing Binding to DNA," *Journal of the American Chemical Society* 111 (1989): 3051–3058, https://doi.org/10.1021/ja00190a046.

21. B. Matter, D. Malejka-Giganti, A. S. Csallany, and N. Tretyakova, "Quantitative Analysis of the Oxidative DNA Lesion, 2,2-Diamino-4-(2-Deoxy-β-d-Erythro-Pentofuranosyl)Amino]-5(2H)-Oxazolone (Oxazolone), In Vitro and In Vivo by Isotope Dilution-Capillary HPLC-ESI-MS/MS," *Nucleic Acids Research* 34 (2006): 5449–5460, https://doi.org/10.1093/nar/gkl596.

22. J. Shao, J. Chen, R. X. Ke, et al., "Enantioselectively Generating Imidazolone dIz by the Chiral DNA Intercalating and 'Light-Switching' Ru(II) Polypyridyl Complex via a Novel Flash-Quench Method," *Free Radical Biology and Medicine* 225 (2024): 157–163, https://doi.org/10.1016/j.freeradbiomed.2024.09.045.

23. E. D. A. Stemp, M. R. Arkin, and J. K. Barton, "Oxidation of Guanine in DNA by $Ru(phen)_2$ $(dppz)^{3+}$ Using the Flash-Quench Technique," *Journal of the American Chemical Society* 119 (1997): 2921–2925, https://doi.org/10.1021/ja963606p.

24. J. Cadet, J.-L. Ravanat, G. R. Martinez, M. H. G. Medeiros, and P. D. Mascio, "Singlet Oxygen Oxidation of Isolated and Cellular DNA: Product Formation and Mechanistic Insights," *Photochemistry and Photobiology* 82 (2006): 1219–1225, https://doi.org/10.1562/2006-06-09-IR-914.

25. T. P. Devasagayam, S. Steenken, M. S. Obendorf, W. A. Schulz, and H. Sies, "Formation of 8-Hydroxy(Deoxy)Guanosine and Generation of Strand Breaks at Guanine Residues in DNA by Singlet Oxygen," *Biochemistry* 30 (1991): 6283–6289, https://doi.org/10.1021/bi00239a029.

26. Y. Rhee, M. R. Valentine, and J. Termini, "Oxidative Base Damage in RNA Detected by Reverse Transcriptase," *Nucleic Acids Research* 23 (1995): 3275–3282, https://doi.org/10.1093/nar/23.16.3275.

27. X. Gong, R. Tao, and Z. Li, "Quantification of RNA Damage by Reverse Transcription Polymerase Chain Reactions," *Analytical Biochemistry* 357 (2006): 58–67, https://doi.org/10.1016/j.ab.2006.06.025.

28. A. Alenko, A. M. Fleming, and C. J. Burrows, "Reverse Transcription Past Products of Guanine Oxidation in RNA Leads to Insertion of A and C Opposite 8-Oxo-7,8-Dihydroguanine and A and G Opposite 5-Guanidinohydantoin and Spiroiminodihydantoin Diastereomers," *Biochemistry* 56 (2017): 5053–5064, https://doi.org/10.1021/acs.biochem.7b00730.

29. J. Flinders, S. C. DeFina, D. M. Brackett, C. Baugh, C. Wilson, and T. Dieckmann, "Recognition of Planar and Nonplanar Ligands in the Malachite Green–RNA Aptamer Complex," *ChemBioChem* 5 (2004): 62–72, https://doi.org/10.1002/cbic.200300701.

30. S. Neubacher and S. Hennig, "RNA Structure and Cellular Applications of Fluorescent Light-up Aptamers," *Angewandte Chemie* 58 (2019): 1266–1279, https://doi.org/10.1002/anie.201806482.

31. J. R. Terrell, T. T. Le, A. Paul, et al., "Structure of an RNA G-Quadruplex From the West Nile Virus Genome," *Nature Communications* 15 (2024): 5428, https://doi.org/10.1038/s41467-024-49761-5.

32. M. Jinek, S. M. Coyle, and J. A. Doudna, "Coupled 5′ Nucleotide Recognition and Processivity in Xrn1-Mediated mRNA Decay," *Molecular Cell* 41 (2011): 600–608, https://doi.org/10.1016/j.molcel.2011.02.004.

33. C. N. Phillips, S. Schowe, C. J. Langeberg, N. Siddique, E. G. Chapman, and M. J. E. Resendiz, "Processing of RNA Containing 8-Oxo-7,8-Dihydroguanosine (8-oxoG) by the Exoribonuclease Xrn-1," *Frontiers in Molecular Biosciences* 8 (2021): 780315, https://doi.org/10.3389/fmolb.2021.780315.

34. S. W. Schowe, C. J. Langeberg, E. G. Chapman, K. Brown, and M. J. E. Resendiz, "Identification of RNA Fragments Resulting From Enzymatic Degradation Using MALDI-TOF Mass Spectrometry," *Journal of Visualized Experiments* 182 (2022): e63720, https://doi.org/10.3791/63720.

35. Y. Li, M. B. Aggarwal, K. Nguyen, K. Ke, and R. C. Spitale, "Assaying RNA Localization In Situ With Spatially Restricted Nucleobase Oxidation," *ACS Chemical Biology* 12 (2017): 2709–2714, https://doi.org/10.1021/acschembio.7b00519.

36. P. Wang, W. Tang, Z. Li, et al., "Mapping Spatial Transcriptome With Light-Activated Proximity-Dependent RNA Labeling," *Nature Chemical Biology* 15 (2019): 1110–1119, https://doi.org/10.1038/s41589-019-0368-5.

37. N. Z. Fantoni, A. H. El-Sagheer, and T. Brown, "A Hitchhiker's Guide to Click-Chemistry With Nucleic Acids," *Chemical Reviews* 121 (2021): 7122–7154, https://doi.org/10.1021/acs.chemrev.0c00928.

38. H. C. Kolb, M. G. Finn, and K. B. Sharpless, "Click Chemistry: Diverse Chemical Function From a Few Good Reactions," *Angewandte Chemie* 40 (2001): 2004–2021, https://doi.org/10.1002/1521-3773(20010601)40:11%3c2004::AID-ANIE2004%3e3.0.CO;2-5.

39. A. K. Leung and P. A. Sharp, "MicroRNA Functions in Stress Responses," *Molecular Cell* 40 (2010): 205–215, https://doi.org/10.1016/j.molcel.2010.09.027.

40. S. A. Mortimer and K. M. Weeks, "Time-Resolved RNA SHAPE Chemistry," *Journal of the American Chemical Society* 130 (2008): 16178–16180, https://doi.org/10.1021/ja8061216.

41. J. E. Ehrhardt and K. M. Weeks, "Time-Resolved, Single-Molecule, Correlated Chemical Probing of RNA," *Journal of the American Chemical Society* 142 (2020): 18735–18740, https://doi.org/10.1021/jacs.0c06221.

42. G. M. Rice, C. W. Leonard, and K. M. Weeks, "RNA Secondary Structure Modeling at Consistent High Accuracy Using Differential SHAPE," *RNA* 20 (2014): 846–854, https://doi.org/10.1261/rna.043323.113.

43. J. Cordes, S. Zhao, C. M. Engel, and J. Stingele, "Cellular Responses to RNA Damage," *Cell* 188 (2025): 885–900, https://doi.org/10.1016/j.cell.2025.01.005.

44. R. C. Spitale, P. Crisalli, R. A. Flynn, E. A. Torre, E. T. Kool, and H. Y. Chang, "RNA SHAPE Analysis in Living Cells," *Nature Chemical Biology* 9 (2013): 18–20, https://doi.org/10.1038/nchembio.1131.

45. A. S. Mironov, I. Gusarov, R. Rafikov, et al., "Sensing Small Molecules by Nascent RNA," *Cell* 111 (2002): 747–756, https://doi.org/10.1016/S0092-8674(02)01134-0.

46. A. Serganov, L. Huang, and D. J. Patel, "Coenzyme Recognition and Gene Regulation by a Flavin Mononucleotide Riboswitch," *Nature* 458 (2009): 233–237, https://doi.org/10.1038/nature07642.

47. A. R. Gruber, R. Lorenz, S. H. Bernhart, R. Neubock, and I. L. Hofacker, "The Vienna RNA Websuite," *Nucleic Acids Research* 36 (2008): W70–W74, https://doi.org/10.1093/nar/gkn188.

48. Y. Ding, A. M. Fleming, and C. J. Burrows, "Sequencing the Mouse Genome for the Oxidatively Modified Base 8-Oxo-7,8-Dihydroguanine by OG-Seq," *Journal of the American Chemical Society* 139 (2017): 2569–2572, https://doi.org/10.1021/jacs.6b12604.

49. N. J. Baird and A. R. Ferré-D'Amaré, "Idiosyncratically Tuned Switching Behavior of Riboswitch Aptamer Domains Revealed by Comparative Small-Angle X-ray Scattering Analysis," *RNA* 16 (2010): 598–609, https://doi.org/10.1261/rna.1852310.

50. Q. Vicens, E. Mondragón, and R. T. Batey, "Molecular Sensing by the Aptamer Domain of the FMN Riboswitch: A General Model for Ligand Binding by Conformational Selection," *Nucleic Acids Research* 39 (2011): 8586–8598, https://doi.org/10.1093/nar/gkr565.

51. W. C. Winkler, S. Cohen-Chalamish, and R. R. Breaker, "An mRNA Structure That Controls Gene Expression by Binding FMN," *PNAS* 99 (2002): 15908–15913, https://doi.org/10.1073/pnas.212628899.

52. J. Chen and J. Stubbe, "Bleomycins: Towards Better Therapeutics," *Nature Reviews Cancer* 5 (2005): 102–112, https://doi.org/10.1038/nrc1547.

Supporting Information

Additional supporting information can be found online in the Supporting Information section.

Supporting File: anie72518-sup-0001-SuppMat.docx